Dyes and Pigments 193 (2021) 109543

Contents lists available at ScienceDirect

Dyes and Pigments

journal homepage: www.elsevier.com/locate/dyepig

Greater miscibility and energy level alignment of conjugated polymers enhance the optoelectronic properties of ternary blend films in organic photovoltaics

Bing Huang Jiang [a,1], Ya-Juan Peng [a,1], Yu-Ching Huang [b], Ru-Jong Jeng [a], Tien-Shou Shieh [c], Ching-I Huang [a,**], Chih-Ping Chen [b,*]

[a] Institute of Polymer Science and Engineering and Advanced Research Center for Green Materials Science and Technology, National Taiwan University, Taipei, 10617, Taiwan
[b] Department of Materials Engineering, Ming Chi University of Technology, New Taipei City, 243, Taiwan
[c] Material and Chemical Research Laboratories, Industrial Technology Research Institute, Hsinchu, 310, Taiwan

ARTICLE INFO

Keywords:
Organic photovoltaic
Ternary blend
Nonfullerene acceptor

ABSTRACT

In this study, we examined the effects of using the p-type conjugated polymers J51 and FATZ as the third component in PM6:Y6–based donor:donor:acceptor (D:D:A) ternary organic photovoltaics (OPVs). We used UV–Vis spectroscopy, photoluminescence spectroscopy, atomic force microscopy, and grazing-incidence wide-angle X-ray scattering to investigate the optoelectronic and morphological properties of the resulting ternary blend films. We evaluated the carrier transport properties of these OPVs to identify the mechanism governing their power conversion efficiencies (PCEs). Of our two tested polymers, FTAZ had more suitable energy levels and miscibility; therefore, its presence increased the open-circuit voltage of the resulting ternary device. The embedded FTAZ facilitated the molecular packing of Y6 and improved the charge transport in the ternary blend, thereby improving the PCE of the device from 14.3% (binary) to 15.3% (ternary).

Introduction

The performance of organic photovoltaics (OPVs) has experienced rapid progress as a result of developments in the design of nonfullerene acceptors (NFAs) [1–7]. The emergence of NFAs has promoted the application of ternary blends to further improve the power conversion efficiencies (PCEs) and stabilities of OPVs [8–12]. The third component can play several roles when incorporated in ternary OPVs. (1) As modifiers of the blend film morphology (i.e., through the effects of miscibility): they can determine whether parallel or alloy models operate within the blends. (2) By providing complementary absorption, they can broaden the range of light harvesting to improve the short-circuit current density (J_{SC}) of the resulting device. (3) By optimizing the energy level alignment of the ternary blends, they can increase the open-circuit voltage (V_{OC}) of the OPV [i.e., through the effect of a third donor (D) or acceptor (A) having a lower-energy highest occupied molecular orbital (HOMO) or a higher-energy lowest unoccupied molecular orbital (LUMO), respectively, relative to their counterparts]. (4) By serving as a morphology-fixing agent to overcome the thermodynamic instability of a bulk-heterojunction (BHJ) nanostructure, thereby improving the long-term stability of the resulting device [13]. Based on these concepts, there is much interest in developing a greater understanding of the factors behind the design of the third component and, thereby, improving the performance of OPVs.

Binary blends of poly[(2,6-(4,8-bis(5-(2-ethylhexyl-3-fluoro)thien-2-yl)-benzo[1,2-*b*:4,5-*b*']dithiophene))–*alt*–(5,5-(1′,3′-di-2-thienyl-5′,7′-bis(2-ethylhexyl)benzo[1′,2′-*c*:4′,5′-*c*']dithiophene-4,8-dione)] (PM6) and 2,2'-((2*Z*,2′*Z*)-((12,13-bis(2-ethylhexyl)-3,9-diundecyl-12,13-dihydro- [1,2,5]thiadiazolo [3,4-e]thieno[2'',3'':4′,5']thieno[2′,3':4,5]pyrrolo[3,2-*g*]thieno[2′,3':4,5]thieno[3,2-*b*]indole-2,10-diyl)bis(methanylylidene))bis(5,6-difluoro-3-oxo-2,3-dihydro-1*H*-indene-2,1-diylidene))dimalononitrile (Y6 or BTP-4F) have been the most studied in the development of high-performance ternary OPVs (Fig. 1a) [14–16]. Although binary PM6:Y6–based OPVs can exhibit outstanding

* Corresponding author.
** Corresponding author.
E-mail addresses: chingih@ntu.edu.tw (C.-I. Huang), cpchen@mail.mcut.edu.tw (C.-P. Chen).
[1] B.H. Jiang and Y.-J. Peng contributed equally to this work.

https://doi.org/10.1016/j.dyepig.2021.109543
Received 7 May 2021; Received in revised form 2 June 2021; Accepted 4 June 2021
Available online 10 June 2021

performance, higher values of J_{SC} and V_{OC} and higher fill factors (FFs) are possible when pursuing a ternary strategy. For instance, the use of a third A material (e.g., ITCPTC, C8-DTC, MeIC, $PC_{71}BM$, or BTP-M) having a higher-energy LUMO (compared with Y6) can lead to optimization of D:A:A blend films; alternatively, employing a third D material (e.g., S3, the terpolymer PM1, or TPD-3F) has promoted the PCEs of PM6:Y6–based OPVs to greater than 17% [5,17–22].

Because of issues related to the miscibility of the third D or A moiety, D:D:A and D:A:A ternary blends can possess complicated blend morphologies. In most scenarios, large-scale phase segregation or severe molecular disorder has appeared in the ternary blends, worsening the performance of the OPVs. Typically, good miscibility (strong intermolecular interactions) among the components of a blend lowers the degree of phase segregation, resulting in smaller domain sizes that benefit charge dissociation. In contrast, weak intermolecular interactions among the components can lead to phase segregation of the blend, potentially facilitating carrier transport through relatively continuous pathways with purer D or A domains. Our goal for this study was to investigate the miscibility of a third D moiety as a means of achieving an optimized well-defined blend morphology, with adequate carrier transport and extraction, in addition to improved light harvesting. Compared with D:A:A OPVs, larger repulsive intermolecular interactions typically exist between the two conjugated D moieties in D:D:A ternary OPVs, leading to infrequent examples of their successful application [17]. As a result, plenty of room remains to develop D:D:A ternary strategies using two conjugated polymers. Here, we evaluated the conjugated polymers poly[(5,6-difluoro-2-octyl-2*H*-benzotriazole-4,7-diyl)-2,5-thiophenediyl[4,8-bis[5-(2-hexyldecyl)-2-thienyl]benzo[1,2-*b*:4,5-*b*']dithiophene-2,6-diyl]-2,5-thiophenediyl] (J51) and poly[(5,6-difluoro-2-(2-butyloctyl)-2*H*-benzotriazole-4,7-diyl)-2,5-thiophenediyl[4,8-bis(3-butylnonyl)benzo[1,2-*b*:4,5-*b*']dithiophene-2,6-diyl]-2,5-thiophenediyl] (FTAZ)—with different miscibilities and energy levels toward PM6—as the third component in a PM6:Y6 binary blend, exploring their optoelectronic properties at various blend ratios (Fig. 1a). With its suitable energy level alignment and miscibility, FTAZ improved the molecular packing of the PM6:Y6 blend film, resulting in the PCE of the OPV increasing from 14.3% (binary) to 15.3% (ternary). Accordingly, this paper provides an example of a new approach for the fabrication of high-performance D:D:A ternary OPV devices.

Results and discussion

We employed the conjugated polymers FTAZ and J51, each having a wide band gap, as the second polymer donor in D:D:A ternary films

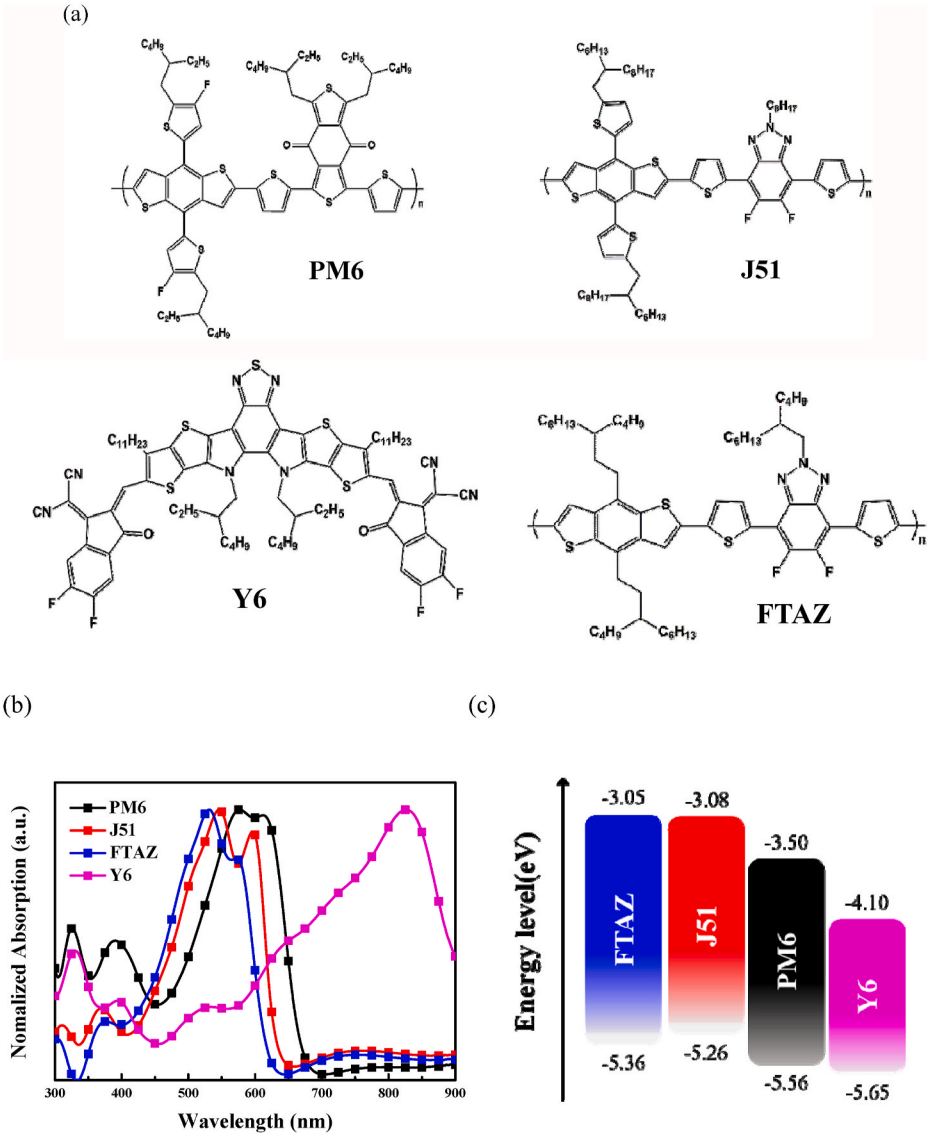

Fig. 1. (a) Chemical structures, (b) thin film absorption spectra, and (c) energy level diagram of PM6, Y6, J51, and FTAZ.

(Fig. 1a). FTAZ was first reported by Price et al., who prepared FTAZ:PCBM and FTAZ:ITIC-Th1 binary devices displaying PCEs of 7.1 and 12.1%, respectively [23–25]. Furthermore, FTAZ:PBDB-T:IT-M– and FTAZ:IDIC:ITIC-TH-S–based ternary blends have been reported with PCEs of 13.2 and 11.6%, respectively [26,27]. Gao and co-workers developed the polymer J51 and demonstrated a high-performance all--polymer J51:N2000 OPV having a PCE of 8.27% [28]. The polymer J51 has also been incorporated into PTB7-Th:ITIC, PTB7-Th:BT-IC, PTB7-Th:N2000, and PBDB-T:ITIC binary blends for evaluation of the resulting ternary OPVs [29–32]. Fig. 1b and c presents the UV–Vis spectra (for films deposited using $CHCl_3$ as solvent) and energy level diagram, respectively, of PM6, Y6, FTAZ, and J51. PM6 absorbs at wavelengths in the range from 300 to 680 nm, with a maximum at 576 nm. J51 and FTAZ are efficient at absorbing light at wavelengths from 300 to 666 nm and from 300 to 650 nm, respectively, with maxima at 530 and 546 nm, respectively. The band gaps of J51 and FTAZ (calculated from the onsets in their absorption spectra) were 1.86 and 1.91 eV, respectively. Thus, the absorptions of J51 and FTAZ covered the visible absorption range well, and they were complementary (maxima at shorter wavelengths) to PM6 [33]. The use of J51 and FTAZ would extend the light available for harvesting to shorter wavelengths, potentially improving the values of J_{SC} of their respective ternary devices. The HOMO/LUMO energy levels of J51 and FTAZ were −3.08/–5.26 and −3.05/–5.36 eV, respectively [23,34]. The different side chains of J51 (alkyl-thiophene) and FTAZ (alkyl) were responsible for their different energy levels. The bulky thiophene unit of J51 affected both the electron-donating properties and the molecular conformation of the main chain, resulting in the HOMO energy level of J51 being slightly higher than that of FTAZ. We expected the cascade of energy levels of J51, FTAZ, PM6, and Y6 to facilitate carrier transport within the ternary blends and, thereby, increase the FFs of their devices. We suspected that efficient exciton dissociation might occur at the J51–PM6, FTAZ–PM6, J51–Y6, and FTAZ–Y6 interfaces. As a result, the presence of J51 and FTAZ as third components in PM6:Y6 ternary blends would lead to cascading energy level alignments and complementary light absorption. Furthermore, because FTAZ and J51 have the same conjugated main chain but different side chains (alkyl thiophene for J51; alkyl for FTAZ), we suspected that the side chains would also play a role affecting the blend film morphology.

We evaluated the Flory–Huggins interaction parameters (χ) of these materials to study their miscibility. We calculated the values of χ using the following equation (where D and A represent the individual donor and acceptor moieties in the blends), with the surface energies (γ) determined from contact angle measurements:

$$\chi\alpha\left(\sqrt{\gamma_D} - \sqrt{\gamma_A}\right)^2$$

The values of χ can be used as a measure of the degree of molecular interaction among the components, and to estimate the resulting BHJ blend film morphology. We used the Wu model (with water and diiodomethane as probe solvents) to determine the contact angles and surface energies of our tested materials [5]. Table 1 lists the surface energies (γ_{total}) and values of χ of the materials; Fig. S1 provides their contact angles. The surface energies of J51, FATZ, PM6, and Y6 were 31.17, 33.69, 38.06, and 47.88 mJ m^{-2}, respectively. Side chain engineering is a main factor affecting the surface energies and miscibilities of material pairs [35]. Here, the different side chains of J51 and FTAZ led to the value of γ_{polar} of J51 being lower than that of FTAZ, with the highly hydrophobic branched alkyl chains on the benzotriazole units of FTAZ leading to its value of $\gamma_{dispersive}$ being higher than that of J51. As a result, the surface energy of FTAZ was higher than that of J51. The values of χ for the J51/PM6, FTAZ/PM6, PM6/Y6, J51/Y6, and FTAZ/Y6 pairs were 0.34, 0.13, 0.56, 1.79, and 1.24, respectively. Thus, the interaction parameters for these materials followed the order J51/Y6 > FTAZ/Y6 > PM6/Y6 > J51/PM6 > FTAZ/PM6. Lower values of χ are indicative of stronger intermolecular interactions and, therefore, improved miscibility for a blend film. From a thermodynamic point of view, without considering the solvent effect (i.e., when fabricating films under the same conditions with evaporation of the same solvent), we predicted that FTAZ would form a well-mixed phase with PM6, whereas J51 might undergo partial phase segregation with PM6. A higher value of $\chi_{D/Y6}$ implies weaker interactions between the donor and Y6, potentially leading to a more phase-segregated BHJ morphology. We followed an approach described in the literature to calculate the wetting coefficients (ω) of our materials and blends [36]. The value of ω can provide some information about the location of the third component within the blend film. A value greater than +1, lower than −1, or between +1 and −1 would suggest that the third component was located in PM6 phase, in the Y6 phase, or at the PM6–Y6 interface, respectively. Our calculated values of ω for J51 and FTAZ in the PM6:Y6 blend film (2.40 and 1.89, respectively) implied that they were presumably located in the PM6 matrix, with different degrees of phase segregation. Although J51 and FTAZ featured the same conjugated main chain, their different side chains (alkyl-thiophene for J51; alkyl for FTAZ) led to variations in their thin-film optoelectronic properties (absorptions, energy levels). One reason for these variations is conformational twisting of the benzodithiophene units, induced by the alkyl-thiophene side chains, in J51. The different side chains also resulted in differences in the molecular packing and surface energies of the thin films, thereby also affecting the miscibility when paired with the other materials.

We fabricated OPVs having the inverted structure indium tin oxide (ITO)/ZnO/BHJ/MoO_3/Ag (Fig. 2). We evaluated the ternary devices using various blend weight ratios. In terms of nomenclature, the OPV incorporating the PM6:J51:Y6 blend (the weight ratio between D and A was fixed at 1:1.2; the concentration was 7.3 mg/mL in $CHCl_3$) having a weight ratio of 0.95:0.05:1.2 is denoted herein, for example, as the 5 wt % J51–ternary OPV. Table 2 and Fig. 2 summarize the performance of the devices. We calculated the average values of the performance data from at least five individual devices. Notably, to avoid the effects of any additives (e.g., chloronaphthalene, which is commonly used to prepare PM6:Y6 binary blends) on the blend film morphology and complicating the discussion, we prepared these OPVs without any additives. The PM6:Y6–based binary device provided a PCE of 14.31 ± 0.16%, with a value of J_{SC} of 25.30 ± 0.08 mA cm^{-2}, a value of V_{OC} of 0.885 ± 0.002 V, and an FF of 65.83 ± 0.38%. These values are similar to those reported previously [5,33]. The 5 wt%–J51 device exhibited a PCE of 11.81 ± 0.02%. Further increasing the content of J51 decreased the PCE of the 10 wt%–J51 OPV to 10.89 ± 0.19%; we attribute the lower PCE, compared with that of the control PM6:Y6 device, mainly to the decrease in the FF from 65.83 ± 0.38 to 54.33 ± 0.90%. In contrast, the 5 wt%–FTAZ ternary OPV had a PCE of 15.30 ± 0.04%, approximately 7% higher than that of the binary OPV, due to the significant increase in the FF from 65.83 ± 0.38 to 69.63 ± 0.16%. The 10 wt%–FTAZ OPV exhibited a PCE of 15.11 ± 0.07%. Fig. S2 reveals that, because of the low weight ratios of J51 and FTAZ, the UV–Vis absorption spectra of these blends were similar, with only small differences in the absorption of Y6. Therefore, theoretically, these OPVs should have provided similar values of J_{SC}. We observed, however, significantly lower values of J_{SC} for the J51-derived devices, suggesting less efficient dissociation or transport of their free carriers. Interestingly, the values of V_{OC} were greater for the FTAZ-containing OPVs, in spite of the higher HOMO energy level of FTAZ (compared with PM6) [5]. This finding suggested that PM6:

Table 1
Surface energies of the materials and values of χ for their blends.

	Surface Energy (γ_{total}) (mJ m^{-2})	Dispersive (γ_d) (mJ m^{-2})	Polar (γ_p) (mJ m^{-2})	χ_{PM6-D}	χ_{Y6-D}	ω
PM6	38.06	36.46	1.60	–	0.56	–
Y6	47.88	43.34	4.54	0.56	–	–
FTAZ	33.69	32.00	1.68	0.13	1.24	1.89
J51	31.17	30.26	0.91	0.34	1.79	2.40

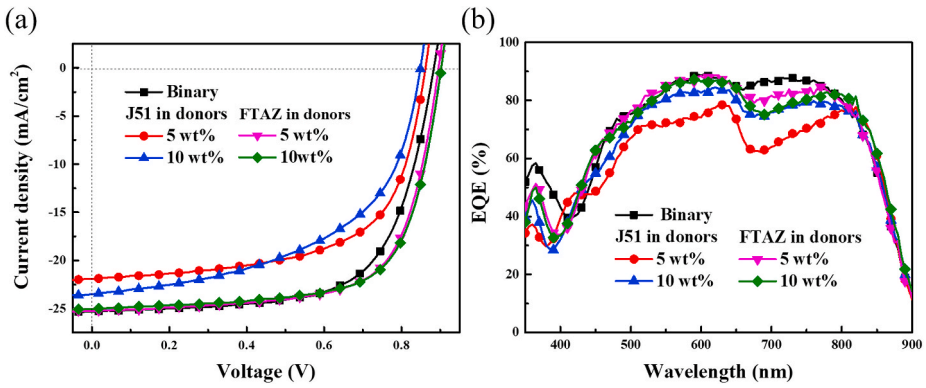

Fig. 2. (a) *J*–*V* and (b) EQE curves of the binary and ternary devices.

Table 2
Device performance of the binary and ternary OPVs.

Composition	J_{SC} (mA cm^{-2})	V_{OC} (V)	FF (%)	PCE (%)	R_{sh} (Ω cm^2)	R_s (Ω cm^2)
Binary	25.30 ± 0.08	0.885 ± 0.002	65.83 ± 0.38	14.31 ± 0.16	573.83	3.42
J51 in donors						
5 wt%	21.83 ± 0.11	0.864 ± 0.002	62.60 ± 0.07	11.81 ± 0.02	437.50	3.26
10 wt%	23.51 ± 0.12	0.853 ± 0.003	54.33 ± 0.90	10.89 ± 0.19	264.41	3.00
FTAZ in donors						
5 wt%	25.06 ± 0.18	0.890 ± 0.007	69.63 ± 0.16	15.30 ± 0.04	619.05	1.75
10 wt%	25.06 ± 0.13	0.895 ± 0.004	68.73 ± 0.45	15.11 ± 0.07	748.89	2.23

FTAZ formed an intermediate energy state having a deeper HOMO energy level, as a result of molecular packing (potentially driven by their miscibility), that enlarged the difference in energy between $HOMO_D$ and $LUMO_{Y6}$ [37,38].

We calculated the shunt (R_{sh}) and series (R_s) resistances from the *J*–*V* curves of the OPVs (Table 2). The largest value of R_{sh} (749 Ω cm^2) and the lowest value of R_s (1.75 Ω cm^2) were those of the 5 wt%–FTAZ ternary OPV, indicating that this device has the lowest leakage current and most efficient charge transport. In comparison with the binary device, the embedding of J51 led to a slight decrease in the value of R_s and a significant decrease in the value of R_{sh}, suggesting that the unsuitable blend morphology or energy level alignment led to a serious leakage current and charge recombination. To support the accuracy of the performance data determined from the solar simulator, we measured the external quantum efficiency (EQE) responses of the binary and J51-and FTAZ-containing ternary devices (Fig. 2b). The calculated values of J_{SC} (from the EQE spectra and the solar flux) of the binary and 5 wt% J51–, 10 wt% J51–, 5 wt% FTAZ–, and 10 wt% FTAZ–containing ternary devices were 24.54, 21.25, 23.03, 24.16, and 24.03 mA cm^{-2}, respectively. Thus, only small mismatches existed between the values of J_{SC} determined from the solar simulator and the EQE responses.

We used tapping-mode atomic force microscopy (AFM) to examine the variations in the blend morphologies governed by the miscibilities of the third components. Fig. 3 presents AFM topographic and phase images of our various blend films. The root-mean-square (RMS) surface roughnesses of the binary and 5 wt% J51–, 10 wt% J51–, 5 wt% FTAZ–, and 10 wt% FTAZ–containing ternary blend films were 3.71, 3.32, 2.99, 4.17, and 2.54 nm, respectively. The incorporation of 5% of J51 and FTAZ changed the surface roughness slightly. Further increasing the content of the third component to 10% decreased the surface roughnesses of both blend films, suggesting that changes had occurred in the molecular packing within these blends [39]. Because the phase images of the blend films were nearly identical, we used grazing-incidence wide-angle X-ray scattering (GIWAXS) to obtain further information. Fig. 4a presents the one-dimensional (1D) GIWAXS profiles of neat PM6, Y6, J51, and FTAZ films recorded along the out-of-plane (OP, red lines) and in-plane (IP, dark lines) directions, extracted from their two-dimensional (2D) diffraction patterns (Fig. S3). The (010) peaks in the OP direction for PM6, Y6, J51, and FTAZ were located at 16.79,

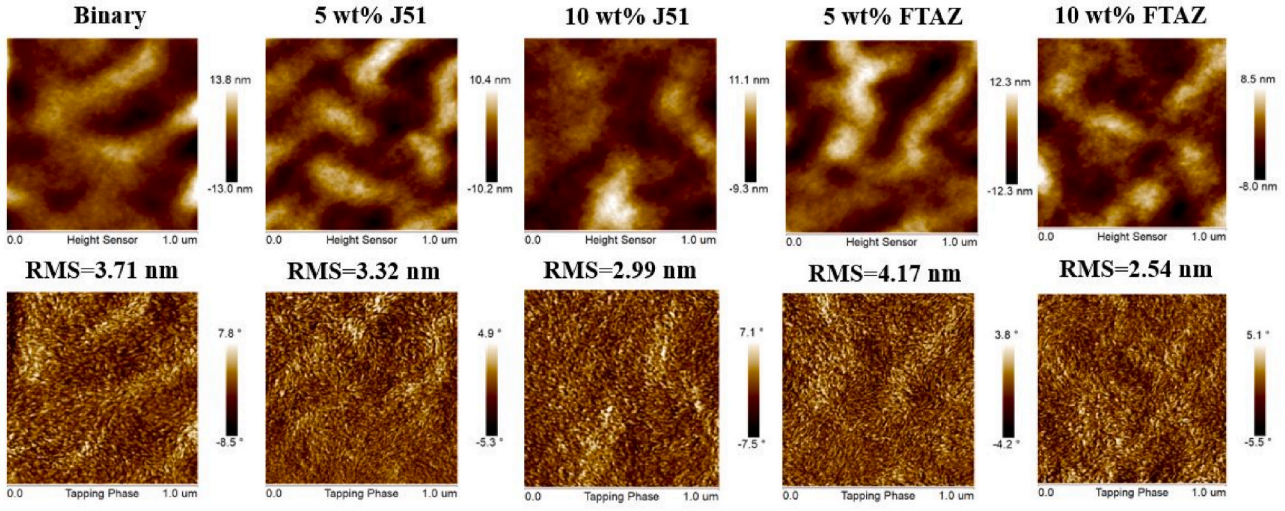

Fig. 3. AFM topographic and phase images of the binary and ternary films.

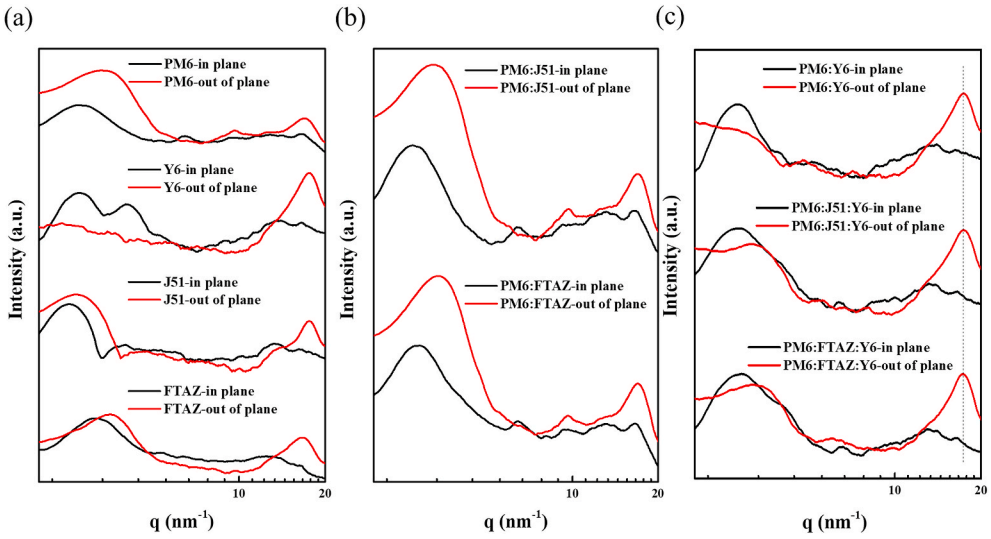

Fig. 4. GIWAXS patterns of the (a) neat films, (b) donor blend films, and (c) binary and ternary blend films.

17.51, 17.63, and 16.73 nm^{-1}, respectively; the corresponding π-stacking distances were 0.374, 0.359, 0.356, and 0.376 nm, respectively. The (100) peak of PM6 in the IP direction was located at 2.74 nm^{-1}, with a corresponding lamellar distance of 2.29 nm. Because of differences in the modes of alkyl–alkyl stacking of their side chains, the lamellar distances of the neat J51 and FTAZ films were 2.45 and 2.00 nm, respectively. All of the diffraction patterns of these neat films are similar to those reported previously [19,32,33,40].

Fig. 4b displays the 1D GIWAXS profiles of the blends of FTAZ and J51 with PM6. The blending of PM6 with J51 or FTAZ did not significantly change its π-stacking distance, indicating that even the addition of 10% of J51 or FTAZ did not change the molecular order of PM6. In contrast, when we introduced FTAZ and J51 into the PM6:Y6 blend film, the (010) diffraction peaks of the ternary blend films in the OP direction were enhanced significantly (Fig. 4c). According to Fig. 4b, we consider the addition of the third component mainly increase the strength of π-stacking between molecules of Y6. This finding is consistent with the enhanced absorption of Y6 (with a slight red-shifting of its absorption peak) in the UV–Vis absorption spectra of its blends (Fig. S2). It has been reported previously that the compatibility of D and A units is highly correlated to their interaction parameter $\chi_{D/A}$ [41]. The higher values of $\chi_{Y6/D}$ for J51 and FTAZ (compared with the value of $\chi_{Y6/PM6}$) suggested lower compatibility between these D units and the A unit, resulting in greater phase separation and enhanced π-stacking of Y6. In addition, we calculated correlation lengths (CLs) using the Scherrer equation:

$$CL = 2\pi k/\triangle q$$

where $\triangle q$ is the full width at half maximum (FWHM) of a diffraction peak. The CLs of the PM6:Y6, PM6:Y6:J51, and PM6:Y6:FTAZ films were 2.35, 2.24, and 2.20 nm, respectively, suggesting that the introduction of the third component did indeed result in the appearance of smaller crystals. Therefore, by improving the molecular packing of Y6, the degrees of charge transport and separation could be enhanced, thereby inhibiting charge recombination.

Because Y6 has great electron affinity, efficient exciton dissociation and charge transfer occur between it and most polymer donors [15,42]. We suspected that the relationship between the exciton dissociation and charge transfer of the D units (herein, PM6:J51 and PM6:FTAZ) might also have governed the device performance of our ternary OPVs [5,43,44]. Thus, we measured the steady-state photoluminescence (PL) spectra of the neat films and those of the blend films containing various amounts of J51 or FTAZ (Fig. 5). When using a wavelength of 550 nm to excite the D units, the values of λ_{max} for the PM6, J51, and FTAZ films were 680, 657, and 638 nm, respectively (Fig. 5). For the PM6:J51 blend film, the emission was localized near 680 nm; its intensity decreased upon decreasing the content of J51. As suggested previously, the light-induced carriers could be transferred from J51 to PM6 through energy transfer (as displayed in Fig. S4) [5,43]. We observed the same phenomenon for the FTAZ blends, but with lower PL intensity in comparison with that of the J51 blends. Notably, the 10 wt% FTAZ/PM6 blend exhibited PL quenching behavior, suggesting that exciton dissociation of PM6 occurred in the sample. Greater charge transfer was possibly one of the reasons for the superior FFs of the FTAZ-containing devices. PL quenching in blends is affected by energy level differences

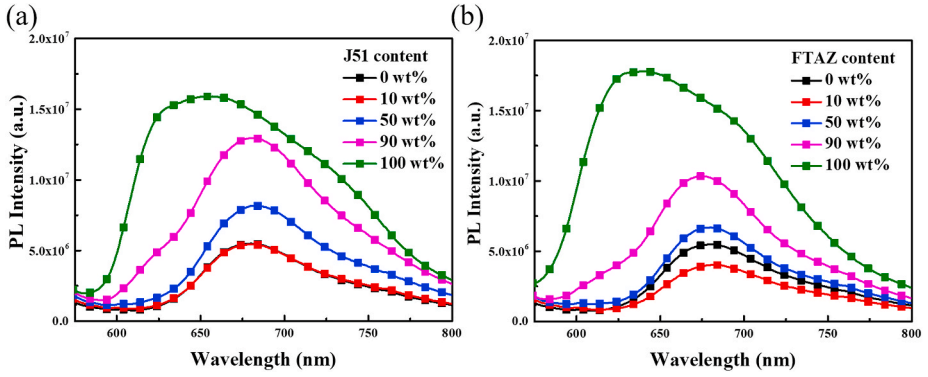

Fig. 5. PL spectra of (a) PM6:J51 and (b) PM6:FTAZ blend films prepared at various ratios.

and film morphologies. Because we did not observe any significant morphological differences or large-area phase segregation in our blends, we conclude that the energy levels of the third component must have played the most important role affecting charge transfer. We fabricated hole-only devices with various D/D ratios to measure their hole mobilities using the space-charge-limited current (SCLC) method, as displayed in Fig. 6a and Fig. S5. The hole mobilities of the neat PM6, 10 wt%–J51/PM6, and 10 wt%–FTAZ/PM6 devices were 4.5×10^{-4}, 4.2×10^{-4}, and 5.1×10^{-4} $cm^2\ V^{-1}\ s^{-1}$, respectively. Thus, an improvement in hole mobility occurred for the FTAZ device, whereas the incorporation of J51 led to a slight decrease in hole mobility, presumably because of its less suitable energy level alignment. Increasing the content of FTAZ or J51 to 50 wt% led to a further decrease in hole mobility, but it increased slightly when present at 90 wt% (compared with each 50 wt% sample). With the exception of the 10% FTAZ blend, the presence of the secondary D unit decreased the hole mobility in these two polymer blends. As suggested by Wu and coworkers, efficient carrier transport will lower the energy loss of a device [45]. The incorporation of FTAZ ensured efficient carrier transport and collection and led to higher values of V_{OC}. Thus, the miscibility, chemical structure, energy levels, and blend ratios of the third component all affected the performance of the respective OPV devices.

We measured the photocurrent density with respect to the effective voltage (J_{ph}–V_{eff}) for our binary and ternary devices to investigate the changes in the maximum amounts of absorbed photons (G_{max}) and the charge extraction probabilities [P(E,T)], calculated using the following equations [46,47].

$$J_{ph} = J_{light} - J_{dark}$$

$$V_{eff} = V_0 - V_a$$

$$J_{sat} = q\ G_{max}\ L$$

$$J_{ph} = q\ G_{max}\ P(E,T)\ L$$

where J_{light} and J_{dark} are the current densities under illumination and in the dark, respectively; V_0 is the voltage when J_{ph} was equal to 0; V_a is the applied voltage; q is the elementary charge; and L is the thickness of the active layer. As revealed in Fig. 6b, at lower values of V_{eff} (<0.1 V), the values of J_{ph} increased rapidly upon increasing the voltage, but became saturated when the value of V_{eff} was greater than 0.2 V. The saturated current density (J_{sat}) was determined when the value of V_{eff} was greater than 2.5 V; Table S1 summarizes the parameters. The values of G_{max} of the binary and 5 wt% J51–, 10 wt% J51–, 5 wt% FTAZ–, and 10 wt% FTAZ–containing ternary devices were 1.65, 1.61, 1.64, 1.63, and 1.65 $\times 10^{28}$ $m^{-3}\ s^{-1}$, respectively. Because of the low loading contents of J51 and FTAZ, their values of G_{max} were similar (G_{max} is highly related to the UV–Vis absorption behavior of blend films). The values of P(E,T) of the binary and 5 wt% J51–, 10 wt% J51–, 5 wt% FTAZ–, and 10 wt% FTAZ–containing ternary devices were 93.84, 88.48, 88.26, 92.73, and 93.88%, respectively. The significant decreases in the values of P(E,T) of the J51-containing ternary devices are consistent with the poor transfer properties of J51 limiting the degree of charge extraction. The embedding of FTAZ did not limit the transportation or extraction of the carriers, as revealed by the values of P(E,T) being similar to those obtained for the binary OPV device.

Finally, we investigated the charge recombination properties of the binary and ternary devices from their J–V curves recorded under light of various intensities. Fig. 6c and d presents the plots of J_{SC} and V_{OC} with respect to the light intensity. We calculated the relationship between J_{SC} and the light intensity by using the equation [47,48].

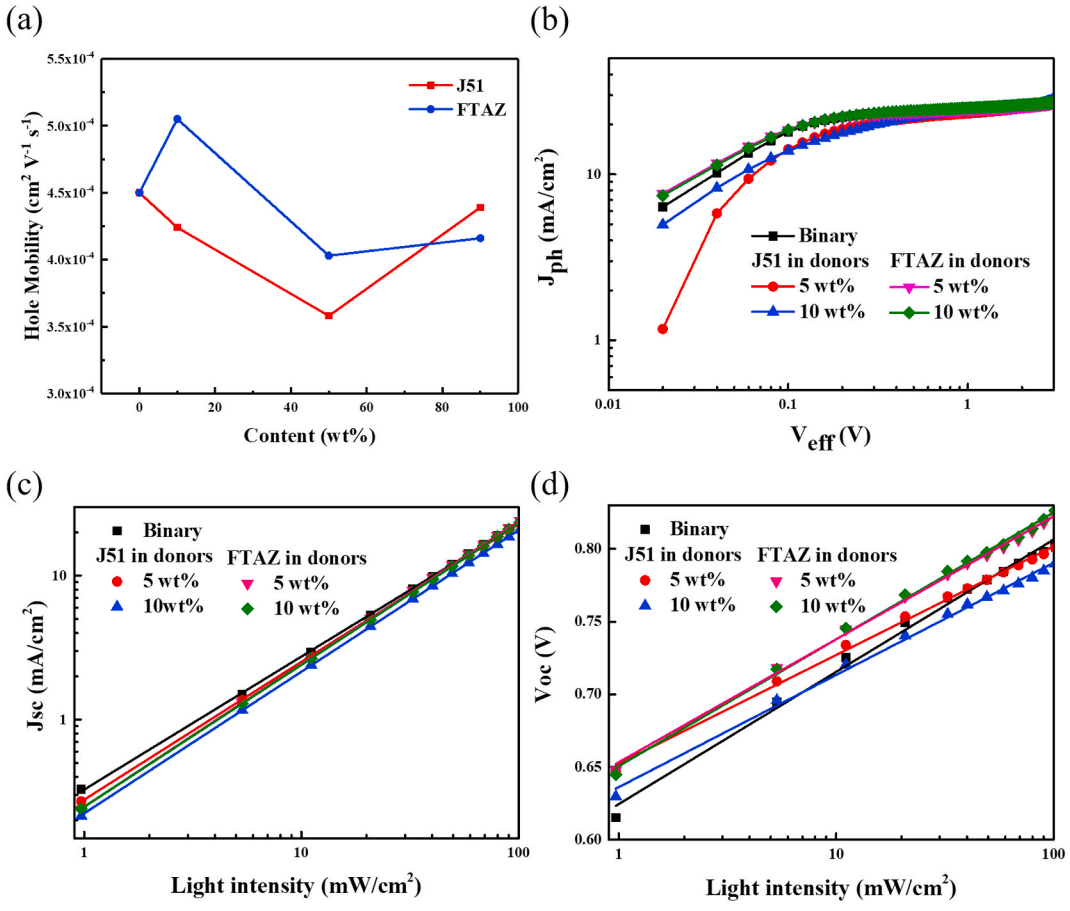

Fig. 6. (a) SCLC hole mobilities of the D blends. (b–d) Plots of (b) J_{ph}–V_{eff}, (c) J_{SC}–light intensity, and (d) V_{OC}–light intensity of the binary and ternary devices.

$$J_{SC} \propto P_{light}^{\alpha}$$

where P_{light} is the power of the light intensity and α is an exponential factor. The fitted values of α for the binary and 5 wt% J51–, 10 wt% J51–, 5 wt% FTAZ–, and 10 wt% FTAZ–containing ternary devices were 0.925, 0.958, 0.985, 0.992, and 0.987, respectively. The embedding of J51 and FTAZ enhanced the value of α, suggesting improvements in bimolecular recombination, presumably because the molecular packing order of the blend film was optimized. Of the two, the presence of FTAZ led to a much greater improvement in the value of α. The same phenomenon has been observed previously for other D:D:A ternary OPVs: Gao and Zhang et al. found that embedding a third component played an important role in suppressing bimolecular recombination and improving device performance [43,49]. The relationship between V_{OC} and the light intensity followed the equation [47,48].

$$V_{OC} \propto n(KT/q)\ln(P_{light})$$

where K is the Boltzmann constant, T is the temperature, q is the elementary charge, and n is a fitted value that can be used to evaluate the degree of trap-assisted recombination. The fitted values of n for the binary and 5 wt% J51–, 10 wt% J51–, 5 wt% FTAZ–, and 10 wt% FTAZ–containing ternary devices were 1.53, 1.26, 1.30, 1.42, and 1.46, respectively. Again, the embedding of J51 and FTAZ improved the degree of trap-assisted recombination, with values of n closer to 1 in comparison with that for the binary OPV device.

The energy levels and the miscibility of the third component both significantly affected the performance of the ternary OPV devices. From the point of view of miscibility, the embedding of J51 and FTAZ enhanced the molecular packing of Y6. Both J51 and FTAZ preferred to distribute in the PM6 matrix without destroying the molecular order of PM6. The enhancement in the order of Y6 resulted in improvements in the degrees of bimolecular and trap-assisted recombination. In the meantime, the HOMO energy level of the third component determined the electronic properties of the mixed D moieties. For example, FTAZ mixed well with PM6 and altered the pseudo-HOMO energy levels (particularly for the 10% FTAZ ternary OPV) to increase the value of V_{OC} and enhance the hole mobility and exciton charge extraction of the device; in contrast, the presence of J51 limited the carrier transport and the value of V_{OC} of its ternary OPVs, due to a larger mismatch in HOMO energy levels. Further detailed investigations will be necessary to provide a clearer understanding of how the offset between the HOMO energy levels of the two D units could improve the values of V_{OC} of ternary OPVs.

Conclusion

We have incorporated the polymer donors J51 and FTAZ as the third blend component in PM6:Y6 ternary OPVs. The energy levels and miscibilities of J51 and FTAZ had significant effects on the molecular packing and charge transfer in the ternary blend films and on their OPV performance. The large difference between the values of $\chi_{Y6/J51}$ (1.79) and $\chi_{J51/PM6}$ (0.34) enhanced the molecular packing of Y6 and affected the energy level alignment of PM6/J51, thereby limiting the carrier transport in those ternary devices. The impeded charge transport and collection in the J51-containing ternary OPVs led to lower values of J_{SC}, V_{OC}, FF, and PCE. The presence of FTAZ also enhanced the molecular packing of Y6 ($\chi_{Y6/FTAZ} = 1.24$), with a low value of $\chi_{FTAZ/PM6}$ (0.13) helping to form a well-mixed FTAZ/PM6 blend that decreased the effective HOMO energy level of the D moieties and increased the value of V_{OC} of its ternary OPVs. The embedding of FTAZ also promoted charge transport and collection and enhanced the FF and PCE—with the latter increasing from 14.3% (binary) to 15.3% (ternary). Thus, we have developed an effective ternary OPV, and provide some guidelines herein for choosing the third component of D:D:A–type ternary OPVs.

Declaration of competing interest

The authors declare that they have no known competing financial interests or personal relationships that could have appeared to influence the work reported in this paper.

Acknowledgment

We thank the Ministry of Science and Technology of Taiwan (MOST 108-2221-E-131-003) for providing financial support.

Appendix A. Supplementary data

Supplementary data to this article can be found online at https://doi.org/10.1016/j.dyepig.2021.109543.

Author contribution statement

Bing Huang Jiang: Validation, Data analysis, Writing - Original Draft. Ya-Juan Peng: Validation, Investigation, Writing - original draft. Yu-Ching Huang: Formal analysis, Writing - review & editing. Ru-Jong Jeng: Resources, Writing - Review & Editing. Tien-Shou Shieh: Resources, Writing - Review & Editing. Ching-I Huang: Conceptualization, Resources, Supervision, Writing - Review & Editing. Chih- Ping Chen: Conceptualization, Methodology, Supervision, Project administration, Resources, Writing - review & editing.

References

[1] Gao W, Fu H, Li Y, Lin F, Sun R, Wu Z, et al. Asymmetric acceptors enabling organic solar cells to achieve an over 17% efficiency: conformation effects on regulating molecular properties and suppressing nonradiative energy loss. Adv Energy Mater.11(4):2003177.
[2] Peng Z, Jiang K, Qin Y, Li M, Balar N, O'Connor BT, et al. Modulation of morphological, mechanical, and photovoltaic properties of ternary organic photovoltaic blends for optimum operation. Adv Energy Mater.11(8):2003506.
[3] Cui Y, Yao H, Zhang J, Xian K, Zhang T, Hong L, et al. Single-Junction organic photovoltaic cells with approaching 18% efficiency. Adv Mater 2020;32(19):1908205.
[4] Luo Z, Ma R, Liu T, Yu J, Xiao Y, Sun R, et al. Fine-tuning energy levels via asymmetric end groups enables polymer solar cells with efficiencies over 17%. Joule 2020;4(6):1236–47.
[5] Jiang B-H, Wang Y-P, Liao C-Y, Chang Y-M, Su Y-W, Jeng R-J, et al. Improved blend film morphology and free carrier generation provide a high-performance ternary polymer solar cell. ACS Appl Mater Interfaces 2021;13(1):1076–85.
[6] Saito M, Tamai Y, Ichikawa H, Yoshida H, Yokoyama D, Ohkita H, et al. Significantly sensitized ternary blend polymer solar cells with a very small content of the narrow-band gap third component that utilizes optical interference. Macromolecules 2020;53(23):10623–35.
[7] Derkowska-Zielinska B, Gondek E, Pokladko-Kowar M, Kaczmarek-Kedziera A, Kysil A, Lakshminarayana G, et al. Photovoltaic cells with various azo dyes as components of the active layer. Sol Energy 2020;203:19–24.
[8] Yang W, Luo Z, Sun R, Guo J, Wang T, Wu Y, et al. Simultaneous enhanced efficiency and thermal stability in organic solar cells from a polymer acceptor additive. Nat Commun 2020;11(1):1218.
[9] Zhang Y, Li G. Functional third components in nonfullerene acceptor-based ternary organic solar cells. Acc Mater Res 2020;1(2):158–71.
[10] Yang T, Ma R, Cheng H, Xiao Y, Luo Z, Chen Y, et al. A compatible polymer acceptor enables efficient and stable organic solar cells as a solid additive. J Mater Chem, A 2020;8(34):17706–12.
[11] Gao H-H, Sun Y, Li S, Ke X, Cai Y, Wan X, et al. An all small molecule organic solar cell based on a porphyrin donor and a non-fullerene acceptor with complementary and broad absorption. Dyes and Pigments 2020;176:108250.
[12] Liu Z, Wang N. Efficient ternary all small molecule organic photovoltaics with NC70BA as third component materials. Dyes and Pigments 2021;187:109111.
[13] Chang L, Sheng M, Duan L, Uddin A. Ternary organic solar cells based on non-fullerene acceptors: a review. Org Electron 2021;90:106063.
[14] Tokmoldin N, Hosseini SM, Raoufi M, Phuong LQ, Sandberg OJ, Guan H, et al. Extraordinarily long diffusion length in PM6:Y6 organic solar cells. J Mater Chem, A 2020;8(16):7854–60.
[15] Guo Q, Guo Q, Geng Y, Tang A, Zhang M, Du M, et al. Recent advances in PM6:Y6-based organic solar cells. Mater Chem Front 2021;5(8):3257–80.
[16] Jiang B-H, Chen C-P, Liang H-T, Jeng R-J, Chien W-C, Yu Y-Y. The role of Y6 as the third component in fullerene-free ternary organic photovoltaics. Dyes and Pigments 2020;181:108613.

[17] Firdaus Y, Le Corre VM, Karuthedath S, Liu W, Markina A, Huang W, et al. Long-range exciton diffusion in molecular non-fullerene acceptors. Nat Commun 2020; 11(1):5220.
[18] Ma X, Wang J, Gao J, Hu Z, Xu C, Zhang X, et al. Achieving 17.4% efficiency of ternary organic photovoltaics with two well-compatible nonfullerene acceptors for minimizing energy loss. Adv Energy Mater 2020;10(31):2001404.
[19] Hultmark S, Paleti SHK, Harillo A, Marina S, Nugroho FAA, Liu Y, et al. Suppressing Co-crystallization of halogenated non-fullerene acceptors for thermally stable ternary solar cells. Adv Funct Mater 2020;30(48):2005462.
[20] Khan MU, Hussain R, Yasir Mehboob M, Khalid M, Shafiq Z, Aslam M, et al. Silico modeling of new "Y-Series"-Based near-infrared sensitive non-fullerene acceptors for efficient organic solar cells. ACS Omega 2020;5(37):24125–37.
[21] Ma R, Liu T, Luo Z, Gao K, Chen K, Zhang G, et al. Adding a third component with reduced miscibility and higher LUMO level enables efficient ternary organic solar cells. ACS Energy Lett 2020;5(8):2711–20.
[22] Wu J, Li G, Fang J, Guo X, Zhu L, Guo B, et al. Random terpolymer based on thiophene-thiazolothiazole unit enabling efficient non-fullerene organic solar cells. Nat Commun 2020;11(1):4612.
[23] Price SC, Stuart AC, Yang L, Zhou H, You W. Fluorine substituted conjugated polymer of medium band gap yields 7% efficiency in polymer− fullerene solar cells. J Am Chem Soc 2011;133(12):4625–31.
[24] Zhao F, Dai S, Wu Y, Zhang Q, Wang J, Jiang L, et al. Single-junction binary-blend nonfullerene polymer solar cells with 12.1% efficiency. Adv Mater 2017;29(18): 1700144.
[25] Liao Z, Xie Y, Chen L, Tan Y, Huang S, An Y, et al. Fluorobenzotriazole (FTAZ)-Based polymer donor enables organic solar cells exceeding 12% efficiency. Adv Funct Mater 2019;29(10):1808828.
[26] Fan B, Zhang D, Li M, Zhong W, Zeng Z, Ying L, et al. Achieving over 16% efficiency for single-junction organic solar cells. Sci China Chem 2019;62(6): 746–52.
[27] Cheng P, Wang J, Zhang Q, Huang W, Zhu J, Wang R, et al. Unique energy alignments of a ternary material system toward high-performance organic photovoltaics. Adv Mater 2018;30(28):1801501.
[28] Gao L, Zhang Z-G, Xue L, Min J, Zhang J, Wei Z, et al. All-polymer solar cells based on absorption-complementary polymer donor and acceptor with high power conversion efficiency of 8.27%. Adv Mater 2016;28(9):1884–90.
[29] Zhang Q, Chen Z, Ma W, Xie Z, Liu J, Yu X, et al. Efficient nonhalogenated solvent-processed ternary all-polymer solar cells with a favorable morphology enabled by two well-compatible donors. ACS Appl Mater Interfaces 2019;11(35):32200–8.
[30] Yu Y-Y, Tsai T-W, Chen C-P. Efficient ternary organic photovoltaics using two conjugated polymers and a nonfullerene acceptor with complementary absorption and cascade energy-level alignment. J Phys Chem C 2018;122(43):24585–91.
[31] Zhong L, Li YX, Bin HJ, Zhang M, Huang H, Hu Q, et al. Ternary polymer solar cells based-on two polymer donors with similar HOMO levels and an organic acceptor with absorption extending to 850 nm. Org Electron 2018;62:89–94.
[32] Zhong L, Gao L, Bin H, Hu Q, Zhang Z-G, Liu F, et al. High efficiency ternary nonfullerene polymer solar cells with two polymer donors and an organic semiconductor acceptor. Adv Energy Mater 2017;7(14):1602215.
[33] Yuan J, Zhang Y, Zhou L, Zhang G, Yip H-L, Lau T-K, et al. Single-Junction organic solar cell with over 15% efficiency using fused-ring acceptor with electron-deficient core. Joule 2019;3:1140–51.
[34] Min J, Zhang Z-G, Zhang S, Li Y. Conjugated side-chain-isolated D–A copolymers based on benzo[1,2-b:4,5-b′]dithiophene-alt-dithienylbenzotriazole: synthesis and photovoltaic properties. Chem Mater 2012;24(16):3247–54.
[35] Lee C, Lee S, Kim G-U, Lee W, Kim BJ. Recent advances, design guidelines, and prospects of all-polymer solar cells. Chem Rev 2019;119(13):8028–86.
[36] An Q, Zhang F, Sun Q, Zhang M, Zhang J, Tang W, et al. Efficient organic ternary solar cells with the third component as energy acceptor. Nano Energy 2016;26: 180–91.
[37] Liu X, Zheng Z, Xu Y, Wang J, Wang Y, Zhang S, et al. Quantifying Voc loss induced by alkyl pendants of acceptors in organic solar cells. J Mater Chem C 2020;8(36): 12568–77.
[38] Xiao B, Zhang M, Yan J, Luo G, Gao K, Liu J, et al. High efficiency organic solar cells based on amorphous electron-donating polymer and modified fullerene acceptor. Nano Energy 2017;39:478–88.
[39] Kekuda D, Lin H-S, Chyi Wu M, Huang J-S, Ho K-C, Chu C-W. The effect of solvent induced crystallinity of polymer layer on poly(3-hexylthiophene)/C70 bilayer solar cells. Sol Energy Mater Sol Cell 2011;95(2):419–22.
[40] Jia T, Zhang J, Zhong W, Liang Y, Zhang K, Dong S, et al. 14.4% efficiency all-polymer solar cell with broad absorption and low energy loss enabled by a novel polymer acceptor. Nano Energy 2020;72:104718.
[41] McDowell C, Abdelsamie M, Toney MF, Bazan GC. Solvent additives: key morphology-directing agents for solution-processed organic solar cells. Adv Mater 2018;30(33):1707114.
[42] Wen Z-C, Yin H, Hao X-T. Recent progress of PM6:Y6-based high efficiency organic solar cells. Surf Interfaces 2021;23:100921.
[43] Xie G, Zhang Z, Su Z, Zhang X, Zhang J. 16.5% efficiency ternary organic photovoltaics with two polymer donors by optimizing molecular arrangement and phase separation. Nano Energy 2020;69:104447.
[44] Yan T, Ge J, Lei T, Zhang W, Song W, Fanady B, et al. 16.55% efficiency ternary organic solar cells enabled by incorporating a small molecular donor. J Mater Chem, A 2019;7(45):25894–9.
[45] Liu S, Yuan J, Deng W, Luo M, Xie Y, Liang Q, et al. High-efficiency organic solar cells with low non-radiative recombination loss and low energetic disorder. Nat Photonics 2020;14(5):300–5.
[46] Jiang B-H, Chan P-H, Su Y-W, Hsu H-L, Jeng R-J, Chen C-P. Surface properties of buffer layers affect the performance of PM6:Y6–based organic photovoltaics. Org Electron 2020;87:105944.
[47] Jiang B-H, Chen C-P, Liang H-T, Jeng R-J, Chien W-C, Yu Y-Y. The role of Y6 as the third component in fullerene-free ternary organic photovoltaics. Dyes Pigments 2020;181:108613.
[48] Wang C-K, Jiang B-H, Lu J-H, Cheng M-T, Jeng R-J, Lu Y-W, et al. A near-infrared absorption small molecule acceptor for high-performance semitransparent and colorful binary and ternary organic photovoltaics. ChemSusChem 2020;13(5): 903–13.
[49] Tang Y, Yu J, Sun H, Wu Z, Koh CW, Wu X, et al. Two compatible polymer donors enabling ternary organic solar cells with a small nonradiative energy loss and broad composition tolerance. Solar RRL 2020;4(11):2000396.